Available online at www.sciencedirect.com

ScienceDirect

Nuclear Physics A 970 (2018) 208–223

NUCLEAR PHYSICS A

www.elsevier.com/locate/nuclphysa

Study of incomplete fusion reaction dynamics in $^{13}C + ^{165}Ho$ system and its dependence on various entrance channel parameters

Suhail A. Tali [a,*], Harish Kumar [a], M. Afzal Ansari [a,*], Asif Ali [a], D. Singh [b], Rahbar Ali [c], Pankaj K. Giri [b], Sneha B. Linda [b], Siddharth Parashari [a], R. Kumar [d], R. P. Singh [d], S. Muralithar [d]

[a] *Department of Physics, Aligarh Muslim University, Aligarh – 202002, India*
[b] *Centre for Applied Physics, Central University of Jharkhand, Ranchi – 835205, India*
[c] *Department of Physics, G. F. (P. G.) College, Shahjahanpur – 242001, India*
[d] *Inter University Accelerator Centre, New Delhi – 110067, India*

Received 30 June 2017; received in revised form 17 November 2017; accepted 17 November 2017
Available online 23 November 2017

Abstract

The excitation functions for the evaporation residues populated in the interaction of $^{13}C + ^{165}Ho$ system have been measured at projectile energies ≈ 4–7 MeV/nucleon. Stacked foil activation technique followed by off-line γ-ray spectroscopy have been employed in the present work. The experimentally measured cross-sections are analyzed in the frame work of statistical model code PACE4, which takes into account only the complete fusion reaction cross-sections. The evaporation residues populated via xn and pxn channels were found to be in good agreement with the PACE4 predictions, while a significant enhancement in the measured cross-sections over PACE4 predictions is observed in case of α-emitting channels, which may be attributed to the incomplete fusion process. For the better understanding of incomplete fusion dynamics, the incomplete fusion fraction has also been deduced and its sensitivity with various entrance channel parameters like: projectile energy, mass-asymmetry, projectile structure in terms of Q_α-value and Coulomb effect has been studied in the present work. The incomplete fusion fraction is found to increase with increasing the projectile energy and a strong projectile structure dependent mass-asymmetry systematic is also observed. The incomplete fusion fraction is also found to be small for more negative Q_α-value projectile (^{13}C) induced reactions as compared to less negative Q_α-value projectiles (^{12}C, ^{16}O and ^{20}Ne) induced

* Corresponding authors.
E-mail addresses: amusuhailtali@gmail.com (S.A. Tali), drmafzalansari@yahoomail.com (M.A. Ansari).

https://doi.org/10.1016/j.nuclphysa.2017.11.012

reactions with the same target nucleus ^{165}Ho. An interesting trend is obtained on further investigation of incomplete fusion dependence on Coulomb effect (Z_PZ_T).

Keywords: Excitation function measurements; Incomplete fusion fraction; Mass-asymmetry; Q_α-value; Coulomb effect

1. Introduction

To understand the complete fusion (CF) and incomplete fusion (ICF) reaction dynamics various efforts have been put-forth, [1–7] since its first observation by Britt and Quinton [8]. Inamura et al. [9] provided the significant information of ICF reaction dynamics from the γ-ray multiplicity measurements. Further, a remarkable and an impressive review of various utmost studies was also summarized by Gerschel [10]. In order to explain the ICF reaction dynamics, various theoretical models have been proposed [11–15], out of which breakup-fusion (BUF) [11] and sum-rule [12] models are mostly used to explain the ICF reaction dynamics. It is important to mention that all the existing models have been able to explain the ICF data at energies $\geq$10 MeV/nucleon. Until now there is no theoretical model available, which could reproduce the ICF data satisfactorily below 8 MeV/nucleon [16,17], hence experimental study of ICF is still an active area of research.

In BUF model, the ICF reaction is explained as a two step process where the incident projectile breaks up into α-clusters (e.g. $^{13}C \rightarrow {}^{9}Be + {}^{4}He(\alpha)$ or $^{5}He + {}^{8}Be(2\alpha)$) in the domain of target nuclear field. The break-up fragments may lead to (a) sequential CF i.e. all the projectile fragments may fuse with the target nucleus and/or (b) one of them may fuse with the target nucleus, while the another fragment moves as a spectator in forward direction with nearly the projectile velocity and have no impact on the way the reaction proceeds. On the other hand, the sum-rule model predicted a specific localization in angular momentum ℓ-space to describe the ICF reaction dynamics. According to sum-rule model approach, the attractive nuclear potential is dominant for $\ell \leq \ell_{crit}$, which may lead to the complete amalgamation of projectile with the target nucleus (i.e. CF) and for $\ell > \ell_{crit}$, there is only ICF process. However, recently some studies have reported signature of ICF process even below $\ell < \ell_{crit}$ [5,7,16,18]. Furthermore Parker et al. [19] observed the ICF features by measuring the forward peaked α-particles in reactions of ^{12}C, ^{15}N, ^{16}O, ^{19}F and ^{20}Ne with ^{51}V target at incident energy of 6 MeV/nucleon. Morgenstern et al. [20] reported that ICF strongly depends on the degree of mass-asymmetry in the entrance channel, which was later on also supported by the other studies [4–7]. However, some recent studies suggested that the Morgenstern's mass-asymmetry systematic is somehow a projectile structure dependent [17,18,21]. Subsequently, ICF dependence on projectile Q_α-value is observed by our group [18] and others [17,21], where the observed projectile structure effect is explored more conclusively. Recently, Shuaib et al. [21] observed a linear growth of ICF with Coulomb effect (Z_PZ_T) only for few projectile–target combinations.

Keeping all the aforementioned views into consideration, the excitation functions (EFs) of various evaporation residues (ERs) populated in the interaction of ^{13}C with ^{165}Ho have been measured and analyzed in the frame work of statistical model code PACE4 [22]. Recent studies based on the EF measurements have shown that ICF also contributes significantly in the formation of ERs [4,7,18,23]. The ICF fraction for present system has been deduced and compared with the data available in the literature for several projectile–target systems as a function of various entrance channel parameters. Presently, projectile structure is found to influence the ICF dynamics and small ICF fraction is observed for ^{13}C (more negative Q_α-value projectile) in comparison to less negative Q_α-value projectiles (^{12}C, ^{16}O and ^{20}Ne) respectively. An attempt has been made to further investigate the ICF dependence on Coulomb effect (Z_PZ_T) and ICF fraction is found to be higher for projectiles ^{20}Ne, ^{16}O and ^{12}C than reactions induced by projectile ^{13}C.

2. Experimental procedure

The experimental work was carried out at Inter University Accelerator Centre (IUAC), New Delhi, India. ^{165}Ho target foils of thickness ≈1.0–1.5 mg/cm^2 and Al-foils having thickness ≈1.5–2.0 mg/cm^2 were fabricated by using the rolling technique. The α-transmission method, which is based on the energy lost by 5.49 MeV α-particles emitted by ^{241}Am source while piercing the target and catcher foils was used to measure the thickness of both target and Al-catcher foils. The Al-foils used, act both as catcher as well as energy degraders. The midpoint energy for each target foil was estimated using the code SRIM08 [24]. Two stacks each consisting of four ^{165}Ho target foils backed by Al-foils were separately irradiated at ≈88 and 71 MeV energies using ^{13}C ion-beam for about 7 hours in General Purpose Scattering Chamber (GPSC), which has an in-vacuum transfer facility (ITF). In order to cover the wide energy range ≈56–88 MeV stacked foil activation technique [25] was employed. A Faraday cup was placed behind the target-catcher assembly to collect the charges, which was further used to calculate the beam flux. The average beam current during the irradiation of both stacks was about 15 nA. After the irradiation of samples, the target-catcher assemblies were dismounted from the GPSC for off-line measurements. The activities induced in each target-catcher foil were recorded by using a pre-calibrated (100 cc) high purity germanium (HPGe) detector coupled to CAMAC-based data acquisition system CANDLE [26].

^{152}Eu γ-source of known strength was used for energy and geometry-dependent efficiency (ε_G) calibration of HPGe detector at various source-detector positions. The distance between irradiated sample and the detector was so adjusted to get sufficient count rate and the dead time of the detector was less than 10%. The ERs populated in the interaction of ^{13}C + ^{165}Ho system were recognized by their characteristic γ-rays and finally confirmed by decay curve analysis, as an example the decay curve of ^{174}Ta is shown in the inset of Fig. 1(a). The observed γ-ray energy spectra obtained at $E_{Lab} \approx 70$ MeV are shown in Fig. 1. The γ-ray peaks have been assigned to the respective ERs populated via emission of xn, pxn, αxn, αpxn and 2αxn channels. It is important to mention that most of the α and 2α emitting channels have longer half-life i.e. in days, thus Fig. 1(b) is the observed energy spectrum at large lapse time with $E_{Lab} \approx 70$ MeV. The populated ERs are listed in Table 1 along with their other spectroscopic properties like half-lives, spin, characteristic γ-ray energies and their branching ratio, which are taken from Refs. [27, 28]. The experimentally measured cross-sections $\sigma(E)$ of ERs was obtained using the following expression [29]:

$$\sigma(E) = \frac{A\lambda \exp(\lambda t_2)}{N_0 \phi I_\gamma K \varepsilon_G [1-\exp(-\lambda t_1)][1-\exp(-\lambda t_3)]} \tag{1}$$

where, A is the total number of counts under the photo-peak, λ is the decay constant of particular ER, t_2 is the time period between beam stop time and counting start time, N_0 is the total number of nuclei present in a target foil, ϕ is the incident beam flux, I_γ is the branching ratio of the characteristic γ-ray, K is the self-absorption correction term for γ-rays, ε_G is the geometry dependent efficiency of the detector, t_1 is the irradiation time and t_3 is the spectra recording

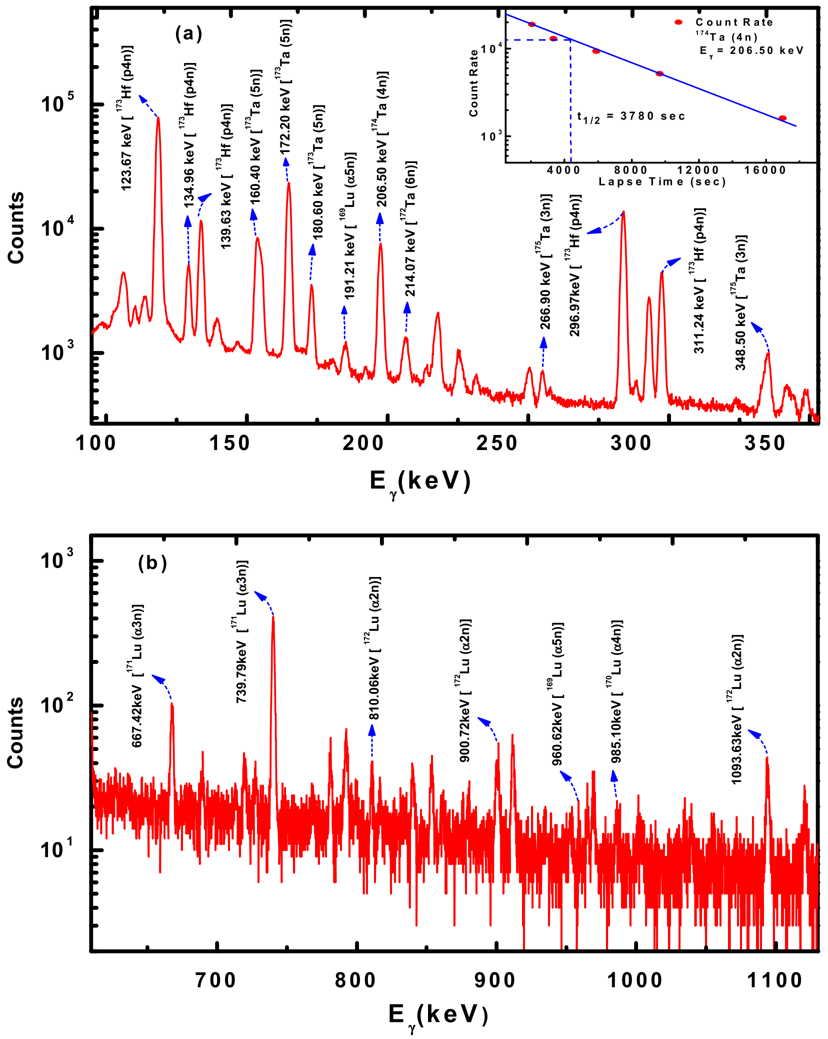

Fig. 1. (Color online.) Typical γ-ray energy spectrum obtained from the interactions of $^{13}C + ^{165}Ho$ system at $E_{lab} = 70$ MeV energy. In the inset of Fig. 1(a), a typical decay-curve for the identification of evaporation residue ^{174}Ta following its half-life.

time. The net possible error in the present work including statistical error was estimated to be less than 15%. Utmost care was taken in determining the quantities such as target thickness, flux measurement and efficiency of HPGe detector, whose inaccurate measurement may introduce errors in the measured cross-sections. Detailed discussion on the error analysis is given in our earlier work [18].

3. Analysis and experimental results

To understand the incomplete fusion reaction dynamics and its dependence on various entrance channel parameters, the excitation functions (EFs) of ERs ^{175}Ta(3n), ^{174}Ta(4n), ^{173}Ta(5n),

Table 1
List of identified evaporation residues populated in $^{13}C + ^{165}Ho$ system via CF and/or ICF, along with their spectroscopic properties.

Reactions	Residues	$T_{1/2}$	J^{π}	E_{γ} (keV)	I_{γ} (%)
^{165}Ho(^{13}C, 3n)	^{175}Ta	10.5 h	7/2$^+$	125.90	5.8
				266.90	10.8
				348.50	12.0
^{165}Ho(^{13}C, 4n)	^{174}Ta	1.05 h	3$^+$	206.50	58.0
				764.79	1.3
				971.06	1.2
^{165}Ho(^{13}C, 5n)	^{173}Ta	3.14 h	5/2$^-$	160.40	4.9
				172.20	18
				180.60	2.2
^{165}Ho(^{13}C, 6n)	^{172}Ta	36.8 min	3$^+$	214.02	55
				1085.58	8.1
				1109.27	14.9
^{165}Ho(^{13}C, p4n)	^{173}Hf	23.6 h	1/2$^-$	123.67	83
				139.63	12.7
				296.97	33.9
				311.24	10.7
^{165}Ho(^{13}C, α2n)	^{172}Lu	6.7 d	4$^-$	810.06	16.6
				900.72	29.8
				1093.66	62.5
^{165}Ho(^{13}C, α3n)	^{171}Lu	8.24 d	7/2$^+$	667.40	11.1
				739.78	47.8
^{165}Ho(^{13}C, α4n)	^{170}Lu	2.01 d	0$^+$	193.13	2.1
				985.10	5.5
^{165}Ho(^{13}C, α5n)	^{169}Lu	34.06 h	7/2$^+$	191.21	20.6
				960.62	23.4
^{165}Ho(^{13}C, αp4n)	^{169}Yb	32.03 d	7/2$^+$	109.78	17.5
^{165}Ho(^{13}C, 2α3n)	^{167}Tm	9.25 d	1/2$^+$	207.80	41
^{165}Ho(^{13}C, 2α4n)	^{166}Tm	7.70 h	2$^+$	705.33	11.0
				778.82	18.9

^{172}Ta(6n), ^{173}Hf(p4n), ^{172}Lu(α2n), ^{171}Lu(α3n), ^{170}Lu(α4n), ^{169}Lu(α5n), ^{169}Yb(αp4n), ^{167}Tm(2α3n) and ^{166}Tm(2α4n) have been measured in the interaction of ^{13}C with ^{165}Ho at $E_{lab} \approx$ 4–7 MeV/nucleon. The independent cross-sections have been deduced following the method suggested by Cavinato et al. [30] and measured EFs are then compared with the theoretical predictions based on statistical model code PACE4 [22]. This code calculates the CF cross-section using Bass formula [31]. The angular momentum projections are calculated at each level of de-excitation, which in-turn makes it possible to determine the angular distribution of emitted particles.

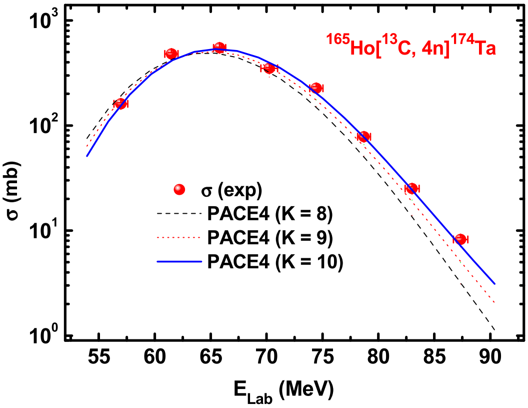

Fig. 2. (Color online.) Comparison of experimentally measured EF of the ER ^{174}Ta populated via 4n channel with theoretical predictions by statistical model code PACE4 for $K = 8, 9, 10$.

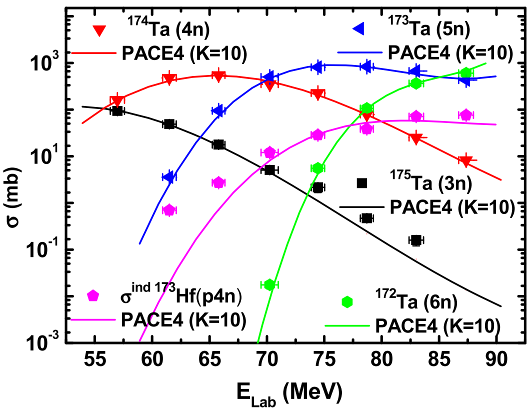

Fig. 3. (Color online.) Experimentally measured EFs of ERs populated via xn (x = 3–6) and pxn (x = 4) channels in the interaction of $^{13}C + ^{165}Ho$ system. The solid lines correspond to the theoretical predictions by statistical model code PACE4 at $K = 10$.

3.1. *Interpretation of xn and pxn channels: only CF process contributes*

In order to reproduce the experimentally measured cross-sections and to choose the suitable level density parameter ($a = A/K$ MeV^{-1}) for analysis of α-emission channels, the free parameter 'K' has been varied from $K = 8$ to 10. As a representative case, the EF of ^{174}Ta populated via emission of 4n channel is shown in Fig. 2. From this figure, it can be seen that experimentally measured cross-sections are well reproduced for $K = 10$. Similarly $K = 10$ has been found to give the best fit for other xn and pxn emission channels as shown in Fig. 3. These ERs are identified on the basis of their half-lives and characteristic γ-ray energies. It is observed that the ER ^{173}Hf ($t_{1/2} = 23.6$ h) populated via p4n channel is strongly fed from its higher-charge precursor isobar ^{173}Ta ($t_{1/2} = 3.14$ h) through an electron capture (EC) process and/or β^+ emission. Using Cavinato et al. [30] formalism, the independent cross-sections of ^{173}Hf (σ^{ind} ^{173}Hf) has been computed (as shown in Fig. 3) from its measured cumulative cross-section as follows:

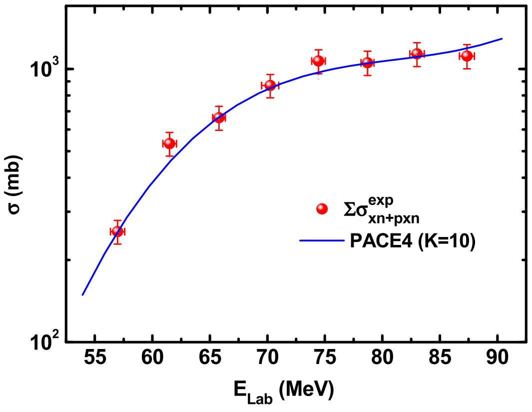

Fig. 4. (Color online.) Sum of experimentally measured EFs of all xn and pxn channels ($\sum \sigma^{\text{exp}}_{xn+pxn}$) are compared with that predicted by statistical model code PACE4 ($\sum \sigma^{\text{PACE4}}_{xn+pxn}$) at $K = 10$.

$$\sigma^{\text{exp}}_{ind}\left(^{173}\text{Hf}\right) = \sigma^{\text{exp}}_{cum}\left(^{173}\text{Hf}\right) - 1.153\sigma^{\text{exp}}_{ind}\left(^{173}\text{Ta}\right) \tag{2}$$

The independent cross-sections of ^{173}Hf well agree with PACE4 predictions for $K = 10$. As mentioned earlier that PACE4 takes into account only CF cross-section, hence it can be concluded that ERs populated via emission of xn and pxn channels are formed as a result of decay of fully equilibrated compound nucleus (CN) ^{178}Ta* i.e. by CF of incident projectile (^{13}C) with target nucleus (^{165}Ho). In Fig. 4, the sum of all experimentally measured xn and pxn channel cross-sections ($\sum \sigma^{\text{exp}}_{xn+pxn}$) has been compared with the theoretical predictions of PACE4 ($\sum \sigma^{\text{PACE4}}_{xn+pxn}$). As can be seen from this figure the theoretical calculations of PACE4 code reproduces well the sum of experimentally measured cross-sections for free parameter $K = 10$. This again supports that these ERs are formed due to the CF of interacting nuclei and level density parameter $a = A/10$ MeV^{-1} is most appropriate for the present work. Same set of input parameters has been retained in PACE4 code for further analysis of α and 2α emitting channels and any enhancement from the theoretical predictions may be accredited to ICF process as proposed by several recent studies [17,18,21,32].

3.1.1. αxn and 2αxn emission channels: accountable for ICF process

The experimentally measured EFs of the ERs populated via emission of α and 2α channels are shown in Figs. 5(a)–5(d) and Figs. 6(a)–6(c), respectively and are compared with the theoretical predictions of PACE4 at level density parameter $a = A/10$ MeV^{-1}. The PACE4 predictions are represented by solid blue curves. As mentioned earlier that PACE4 gives the CF cross-section only, hence any enhancement in the measured cross-sections from the theoretical predictions of PACE4 is ascribed to ICF process. Due to involvement of α and 2α particles emission in the exit channels, there is a possibility that these ERs may be produced from both CF and/or ICF processes. In CF process, the incident projectile (^{13}C) entirely fuses with the target nucleus (^{165}Ho) and forms a fully equilibrated CN (^{178}Ta*), which may further de-excite via n, p, αxn and/or 2αxn emission channels. On the other hand in ICF process, the incident projectile breaks into two fragments in the realm of target nuclear field, only one of the fragments fuses with the target nucleus while the other moves as a spectator in the forward direction. It may be observed form these figures, that the experimentally measured cross-sections show considerable enhancement over the theoretical predictions of PACE4, indicating the presence of ICF along with CF over the

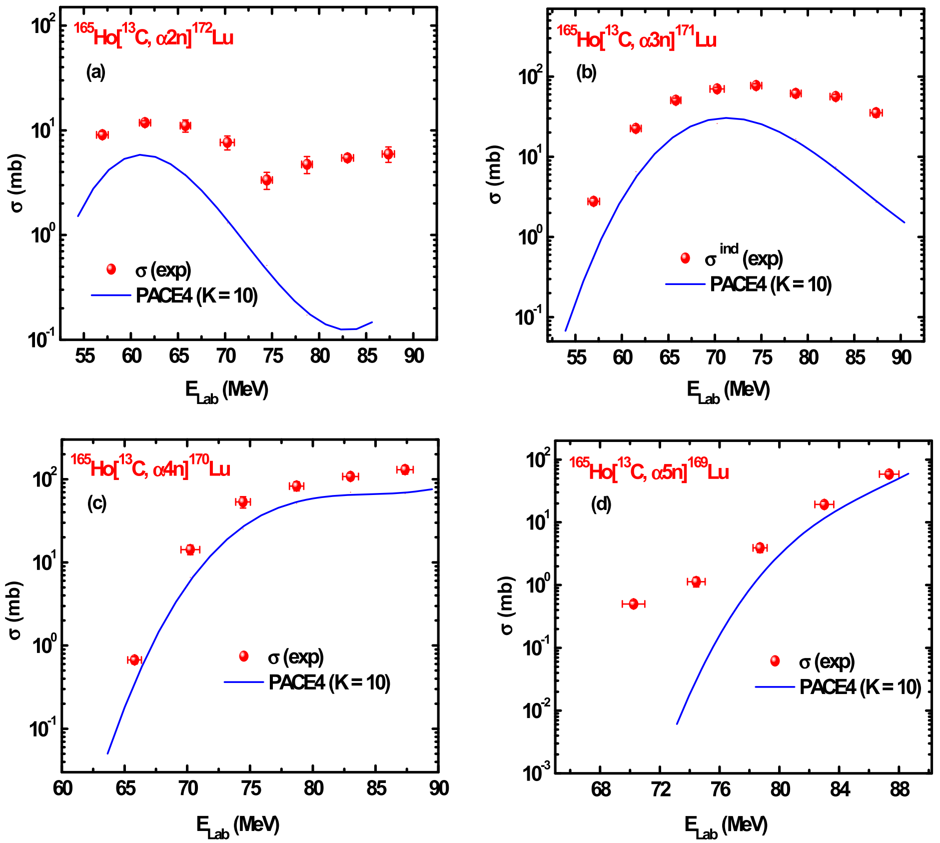

Fig. 5. (Color online.) Experimentally measured EFs of ERs ^{172}Lu(α2n), ^{171}Lu(α3n), ^{170}Lu(α4n) and ^{169}Lu(α5n) populated in the interactions of ^{13}C + ^{165}Ho system. The solid lines correspond to the theoretical predictions by statistical model code PACE4 at $K = 10$.

entire projectile energy range. It may also be observed, that these EF graphs show different trends depending on the ER populated. However ^{172}Lu populated via α2n channel shows an interesting trend which reflects the population of this residue via three different decay channels.

(i) CF-1: the excited CN ^{178}Ta* may decay via emission of two protons and four neutrons (2p4n channel) as

$$^{13}\text{C} + {}^{165}\text{Ho} \Rightarrow {}^{178}\text{Ta}^* \Rightarrow {}^{172}\text{Lu} + 2p4n \ (\text{Q-value} = -51.90\ \text{MeV})$$

(ii) CF-2: the excited CN ^{178}Ta* may decay via emission of an α-particle and two neutrons (α2n channel) as

$$^{13}\text{C} + {}^{165}\text{Ho} \Rightarrow {}^{178}\text{Ta}^* \Rightarrow {}^{172}\text{Lu} + \alpha 2n \ (\text{Q-value} = -23.60\ \text{MeV})$$

(iii) ICF: the excited composite system formed in the break-up of ^{13}C may decay via emission of two neutrons as

$$^{13}\text{C}\left({}^{9}\text{Be} + \alpha\right) + {}^{165}\text{Ho} \Rightarrow {}^{174}\text{Lu}^* \Rightarrow {}^{172}\text{Lu} + 2n \ (\text{Q-value} = -12.95\ \text{MeV})$$

(α-particle moves as spectator)

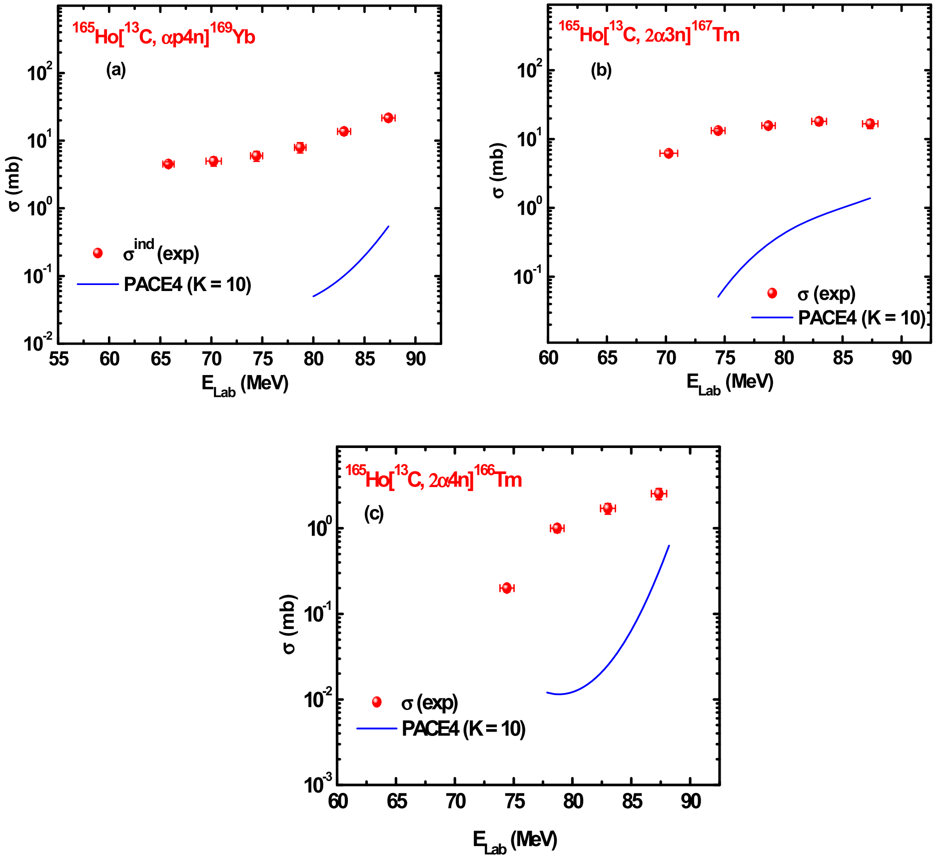

Fig. 6. (Color online.) Experimentally measured EFs of ERs ^{169}Yb(αp4n), ^{167}Tm(2α3n) and ^{166}Tm(2α4n) populated in the interactions of $^{13}C + {}^{165}Ho$ system. The solid lines correspond to the theoretical prediction by statistical model code PACE4 at $K = 10$.

It may be seen from Fig. 5(a), the contributions due to CF-1 and CF-2 reaches at highest point at ≈ 62 MeV. However, for projectile energies at and above ≈ 74 MeV the PACE4 highly underestimates the experimental cross-sections. This shows that ICF remarkably contributes in the formation of ER ^{172}Lu especially at higher energy side.

Further, it is important to mention that the ER ^{171}Lu ($t_{1/2} = 8.24$ d) shown in Fig. 5(b) populated via emission of α3n channel has contribution in its cross-section only at higher energy side coming from the decay of higher charge precursor isobars ^{171}Ta ($t_{1/2} = 23.3$ min) and ^{171}Hf ($t_{1/2} = 12.1$ h). The independent cross-section has been calculated in the same manner using Cavinato et al. [30] formalism and expression for precursor subtraction is as follows:

$$\sigma_{ind}^{exp}\left({}^{171}\mathrm{Lu}\right) = \sigma_{cum}^{exp}\left({}^{171}\mathrm{Lu}\right) - 1.065\sigma_{ind}^{\mathrm{PACE4}}\left({}^{171}\mathrm{Hf}\right) - 1.068\sigma_{ind}^{\mathrm{PACE4}}\left({}^{171}\mathrm{Ta}\right) \tag{3}$$

Also, in case of ^{169}Yb ($t_{1/2} = 32.02$ d) populated via emission of αp4n channel there is a contribution from the decay of its higher charge precursor ^{169}Lu ($t_{1/2} = 34.06$ h), the independent cross-sections has been calculated from its cumulative cross-sections and is shown in Fig. 6(a). The independent cross-sections have been evaluated using the following expression:

$$\sigma_{ind}^{exp}\left(^{169}\text{Yb}\right) = \sigma_{cum}^{exp}\left(^{169}\text{Yb}\right) - 1.05\sigma_{ind}^{exp}\left(^{169}\text{Lu}\right) \tag{4}$$

The EFs for ERs ^{167}Tm(2α3n) and ^{166}Tm(2α4n) are shown in Figs. 6(b) and 6(c). The observed significant enhancement from the PACE4 predictions clearly reveals that these ERs are populated via ICF along with CF. Moreover the reaction mechanism involved in formation of the residues produced via α and 2α emission may be represented as:

1α-emission case:

(i) CF of ^{13}C with ^{165}Ho i.e.

$$^{13}\text{C} + {}^{165}\text{Ho} \Rightarrow {}^{178}\text{Ta}^*$$
$$^{178}\text{Ta}^* \Rightarrow {}^{174-x}\text{Lu} + \alpha + xn \ (x = 2, 3, 4, 5)$$

(ii) ICF of ^{13}C with ^{165}Ho i.e.

$$^{13}\text{C}\left(^{9}\text{Be} + \alpha\right) + {}^{165}\text{Ho} \Rightarrow {}^{174}\text{Lu}^* + \alpha \quad (\alpha \text{ particle moves as a spectator})$$
$$^{174}\text{Lu}^* \Rightarrow {}^{174-x}\text{Lu} + xn \ (x = 2, 3, 4, 5)$$

2α-emission case:

(i) CF of ^{13}C with ^{165}Ho i.e.

$$^{13}\text{C} + {}^{165}\text{Ho} \Rightarrow {}^{178}\text{Ta}^*$$
$$^{178}\text{Ta}^* \Rightarrow {}^{170-x}\text{Tm} + 2\alpha + xn \ (x = 3, 4)$$
$$(\text{Q-value} = -28.29 \text{ MeV and } 37.02 \text{ MeV for } x = 3, 4 \text{ respectively})$$

(ii) ICF of ^{13}C with ^{165}Ho e.g.

$$^{13}\text{C}\left(^{8}\text{Be} + {}^{5}\text{He}\right) + {}^{165}\text{Ho} \Rightarrow {}^{170}\text{Tm}^* + {}^{8}\text{Be} \quad (^{8}\text{Be moves as spectator})$$
$$^{170}\text{Tm}^* \Rightarrow {}^{170-x}\text{Tm} + xn \ (x = 3, 4)$$
$$(\text{Q-value} = -15.34 \text{ MeV and } 24.06 \text{ MeV for } x = 3, 4 \text{ respectively})$$

For better comprehension of ICF contribution, the summation of experimentally measured cross-sections of all α and 2α emitting channels ($\sum \sigma_{\alpha xn+2\alpha xn}^{exp}$) is compared with that evaluated by statistical model code PACE4 ($\sum \sigma_{\alpha xn+2\alpha xn}^{PACE4}$) and is shown in Fig. 7(a). As can be seen from this figure, the experimentally measured cross-sections are notably higher than those predicted by PACE4 code for the same value of level density parameter ($a = A/10$ MeV^{-1}). This enhancement from the theoretical predictions points towards the presence of ICF process in the formation of these ERs. The contribution of ICF in the formation of all α and 2α emitting channels has been calculated as $\sum \sigma_{ICF} = \sum \sigma_{\alpha xn+2\alpha xn}^{exp} - \sum \sigma_{\alpha xn+2\alpha xn}^{PACE4}$. In order to extract more information regarding how ICF contributes to total fusion reaction cross-section ($\sigma_{TF} = \sum \sigma_{CF} + \sum \sigma_{ICF}$), the sum of CF cross-sections of all channels ($\sum \sigma_{CF}$) and σ_{TF} is plotted against incident projectile energy in Fig. 7(b). It is clear from this figure that the separation between σ_{TF} and $\sum \sigma_{CF}$ continuously increases with increase in projectile energy, implying the significant ICF contribution along with CF throughout the energy region of interest. Furthermore, for better visualization of ICF contribution, $\sum \sigma_{ICF}$ with projectile energy is plotted in the inset of Fig. 7(b). The increment in ICF may be due to the fact that break-up probability of the incident projectile ^{13}C into α-clusters [^{9}Be + ^{4}He(α)] and/or [^{5}He + ^{8}Be(2α)] increases as the projectile energy increases.

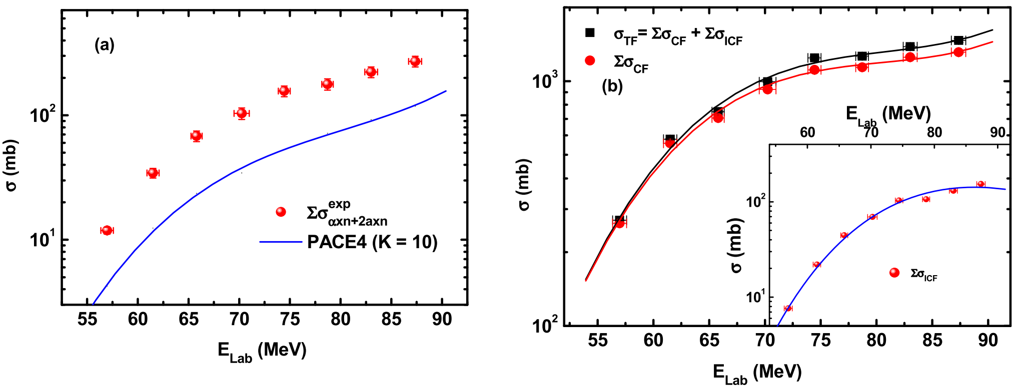

Fig. 7. (Color online.) (a) Comparison of experimentally measured EFs of all αxn+2αxn channels ($\sum\sigma^{exp}_{\alpha xn+2\alpha xn}$) with PACE4 predictions ($\sum\sigma^{PACE4}_{\alpha xn+2\alpha xn}$) at $K = 10$. (b) The total fusion cross section (σ_{TF}), the sum of all CF ($\sum\sigma_{CF}$) and ICF ($\sum\sigma_{ICF}$) channels are plotted as a function of incident projectile energy. The solid lines through the data points are just to guide the eyes.

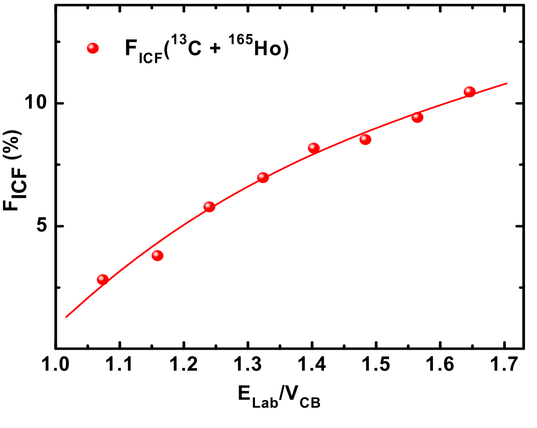

Fig. 8. (Color online.) The deduced F_{ICF} (%) for $^{13}C + ^{165}Ho$ system as a function of reduced incident projectile energy (E_{Lab}/V_{CB}). The line drawn is just to guide the eyes.

In order to understand the dependence of ICF on various entrance channel parameters, the ICF fraction (F_{ICF}) for the presently studied system $^{13}C + ^{165}Ho$ has been estimated as:

$$F_{ICF}(\%) = \frac{\sum\sigma_{ICF}}{\sum\sigma_{CF} + \sum\sigma_{ICF}} \times 100 \tag{5}$$

The calculated F_{ICF} is plotted as a function of Coulomb barrier (V_{CB}) independent projectile energy (E_{Lab}/V_{CB}) and is shown in Fig. 8. From this figure, the value of F_{ICF} was found to be $\approx$3% at projectile energy 7% above V_{CB} and increases up to $\approx$11% at energy 65% above V_{CB}. This increment in F_{ICF} with E_{Lab}/V_{CB} infers that break-up probability of projectile increases with increase in incident energy and also supports the previously observed projectile energy dependent systematic of ICF [5,7,18,32].

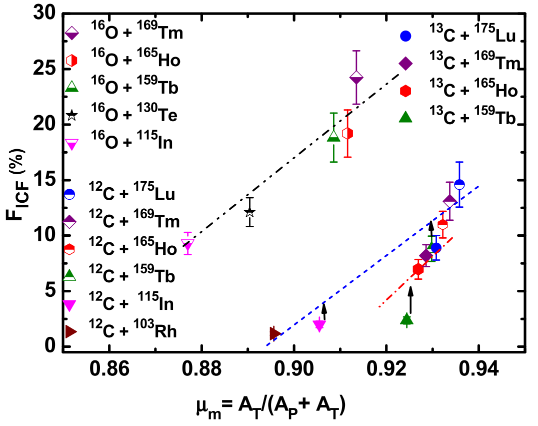

Fig. 9. (Color online.) Comparison of deduced F_{ICF} (%) of $^{13}C+^{165}Ho$ system with earlier studied systems as a function of entrance channel mass-asymmetry (μ_m) at same relative velocity ($v_{rel} \approx 0.053c$). For references see text.

3.1.2. *Effect of mass-asymmetry on ICF*

Mass-asymmetry systematic of Morgenstern et al. [20] has also been further studied in the present work. To have the better visualization of ICF behavior with mass-asymmetry [$\mu_m = A_T/(A_P + A_T)$], the deduced ICF fraction (F_{ICF}) for present system $^{13}C + ^{165}Ho$ has been compared with those obtained for ^{13}C induced reactions with ^{175}Lu [18], ^{169}Tm [33] and ^{159}Tb [32] targets, ^{12}C induced reactions with ^{175}Lu [18], ^{169}Tm [39], ^{165}Ho [37], ^{159}Tb [40], ^{115}In [41] and ^{103}Rh [42] targets and ^{16}O induced reactions with ^{169}Tm [38], ^{165}Ho [17], ^{159}Tb [36], ^{130}Te [35] and ^{115}In [34] targets at same relative velocity ($v_{rel} \approx 0.053c$) and plotted against μ_m in Fig. 9. An interesting trend is observed in this figure and F_{ICF} is found to increase with increasing the mass-asymmetry but separately for each projectile (i.e. ^{12}C, ^{13}C and ^{16}O) with different targets. The present results show deviation from the Morgenstern's mass-asymmetry systematic, where a simple linear growth in F_{ICF} with mass-asymmetry was proposed. This figure quite infers that projectile structure also governs the strength of F_{ICF} in the concerned energy region. Present results are also found to support the recently observed projectile structure dependent mass-asymmetry systematic by our group [18] and others [17,21]. Furthermore, the observed projectile structure effect using α- and non-α-projectiles is interpreted in terms of Q_α-value of projectile and discussed more clearly in next section of this paper.

3.1.3. *Effect of* Q_α*-value on ICF*

To understand the notable behavior of ICF with mass-asymmetry systematic using α- and non-α-cluster structured projectiles and to know how Q_α-value of the projectile governs the ICF reaction dynamics, the deduced ICF fraction (F_{ICF}) for presently studied $^{13}C + ^{165}Ho$ system has been compared along with previously studied systems $^{12}C + ^{165}Ho$ [37], $^{16}O + ^{165}Ho$ [17] and $^{20}Ne + ^{165}Ho$ [5] at same relative velocity $0.053c$, and is shown in Fig. 10. The Q_α-value for projectiles ^{13}C, ^{12}C, ^{16}O and ^{20}Ne are as follows:

$$^{13}C \Rightarrow {}^{9}Be + \alpha, \;\; Q_\alpha = -10.65 \text{ MeV}$$

$$^{12}C \Rightarrow {}^{8}Be + \alpha, \;\; Q_\alpha = -7.37 \text{ MeV}$$

$$^{16}O \Rightarrow {}^{12}C + \alpha, \;\; Q_\alpha = -7.16 \text{ MeV}$$

$$^{20}Ne \Rightarrow {}^{16}O + \alpha, \;\; Q_\alpha = -4.73 \text{ MeV}$$

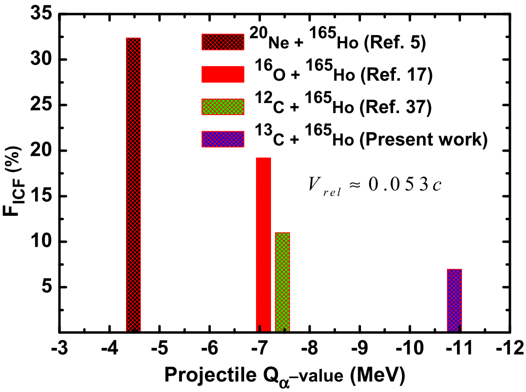

Fig. 10. (Color online.) Comparison of deduced F_{ICF} (%) in terms of Q_α-value of the projectiles at constant relative velocity ($v_{rel} \approx 0.053c$), for ^{13}C, ^{12}C, ^{16}O and ^{20}Ne projectiles with the same ^{165}Ho target.

It is quite clear from this figure that projectiles ^{20}Ne, ^{16}O and ^{12}C having less negative Q_α-value show more ICF fraction compared to more negative Q_α-value projectile ^{13}C. This may be understood in terms of cluster structure of the projectile, since ^{20}Ne, ^{16}O and ^{12}C are well known α-cluster nuclei and have lower Q_α-values compared to ^{13}C. This probably makes ^{13}C more tightly bound and thus has less probability to break-up into clusters nearby the target nuclear field in comparison to other projectiles ^{20}Ne, ^{16}O and ^{12}C. From this figure, it may also be inferred that Q_α-value seems to be an important entrance channel parameter, which plays utmost role in ICF reaction dynamics and explains the projectile structure effect more effectively. Subsequently, the observed projectile structure effect in terms of Q_α-value supports the recent findings obtained by others [17,18,21].

3.1.4. *Effect of Coulomb effect ($Z_P Z_T$) on ICF*

In the present work, the linear growth in ICF fraction with Coulomb effect ($Z_P Z_T$) observed by Shuaib et al. [21] is also further investigated. In order to have the better insight into the $Z_P Z_T$ influence on ICF, the deduced ICF fraction F_{ICF} for the present system $^{13}\text{C} + {}^{165}\text{Ho}$ has been compared with that obtained for previously studied systems [5,17,18,32–42] at same $v_{rel} \approx 0.053c$, as shown in Fig. 11. This figure shows clearly that F_{ICF} values obtained for ^{12}C, ^{16}O and ^{20}Ne induced reactions increase with increasing the parameter $Z_P Z_T$ and lie on the same line. However, the ^{13}C induced reactions with same targets as used for ^{12}C induced reactions have the lower F_{ICF} values. Present observations reveals that Coulomb effect ($Z_P Z_T$) governs the ICF probability only up to some extent and for the interaction of projectiles having same Z_P number like ^{12}C, ^{13}C with the target of same Z_T, the ICF dependence on Coulomb effect is inexplicable. Moreover, the observed discrepancy in ICF dependence on $Z_P Z_T$ using the same Z_P numbered projectiles with the target of same Z_T may be understood more clearly in terms of projectile Q_α-value as represented in Fig. 10. More and more data are needed to reach on some definite conclusions regarding the effect of Coulomb repulsion ($Z_P Z_T$) on ICF in the energy region of 4–7 MeV/nucleon.

4. Summary and conclusions

In the present work, EFs of twelve ERs ^{175}Ta(3n), ^{174}Ta(4n), ^{173}Ta(5n), ^{172}Ta(6n), ^{173}Hf(p4n), ^{172}Lu(α2n), ^{171}Lu(α3n), ^{170}Lu(α4n), ^{169}Lu(α5n), ^{169}Yb(αp4n), ^{167}Tm(2α3n) and ^{166}Tm(2α4n)

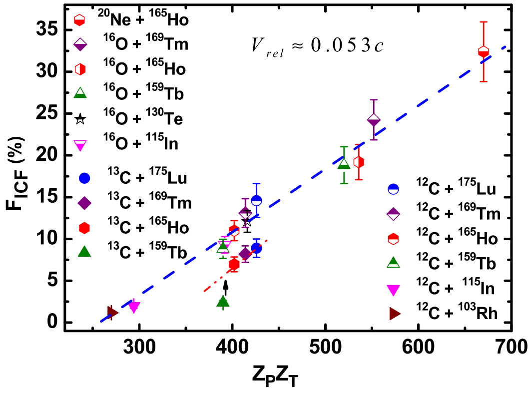

Fig. 11. (Color online.) Comparison of deduced F_{ICF} (%) of $^{13}C + ^{165}Ho$ system with earlier studied systems as a function of entrance channel $Z_P Z_T$ at same relative velocity ($v_{rel} \approx 0.053c$). For references see text.

have been measured for $^{13}C + ^{165}Ho$ system in the energy range of ≈ 4–7 MeV/nucleon. The independent cross-sections in ^{173}Hf, ^{171}Lu and ^{169}Yb populated via p4n, α3n and αp4n channels respectively have been extracted from the higher charge precursor isobars by using Cavinato et al. [30] formalism. A good agreement for experimentally measured xn and pxn channel cross-sections is observed on comparing with theoretical predictions of statistical model code PACE-4 at level density parameter $a = A/10$ MeV^{-1}, indicating the population of these ERs via CF process. However, the ICF is also an important mode of reaction along with CF process in the population of α and 2α emission channels between 4–7 MeV/nucleon energies. Also, the projectile break-up probability is found to increase with increment in the energy of the projectile. The increase in the ICF fraction with mass-asymmetry is observed to increase separately for each projectile with different targets. Furthermore, Q_α-value of the projectile is also found to strongly influence the ICF fraction and relatively higher F_{ICF} value for less negative Q_α-value projectiles is observed compared to more negative Q_α-value projectile. An interesting trend observed in the re-investigation of the ICF dependence on Coulomb effect ($Z_P Z_T$) reveals that the ICF fractions for ^{12}C, ^{16}O and ^{20}Ne induced reactions lie on the same line and are relatively higher in comparison to ^{13}C induced reactions with the targets used as that for ^{12}C. Hence, the present findings are in contrary to Shuaib et al. [21] suggestions, where a simple linear growth in ICF fraction with ($Z_P Z_T$) was reported. Moreover, the present work would be fruitful in understanding and perfect modeling of ICF dynamics in the energy range of 4–7 MeV/nucleon.

Acknowledgements

The authors are grateful to Director IUAC, New Delhi and Chairperson Department of Physics AMU, Aligarh, India for providing the necessary facilities to carry out this work. We are also thankful to Dr. Md. Moin Shaikh for valuable discussions related to this article. One of the author SAT is thankful to DST (India) for providing JRF under DST PURSE Programme. HK also extends his appreciation towards UGC-DAE-CSR, Kolkata for awarding Project Fellowship under its Project UGC-DAE-CSR-KC/CRS/13/NP01 sanctioned to Prof. M. Afzal Ansari.

References

[1] Richard Kaufmann, Richard Wolfgang, Phys. Rev. 121 (1961) 192.

[2] B.S. Tomar, A. Goswami, G.K. Gubbi, A.V.R. Reddy, S.B. Manohar, Phys. Rev. C 58 (1998) 3478.
[3] B. Bindu Kumar, S. Mukherjee, S. Chakrabarty, B.S. Tomar, A. Goswami, S.B. Manohar, Phys. Rev. C 57 (1998) 743.
[4] K. Surendra Babu, R. Tripathi, K. Sudarshan, B.D. Shirvastava, A. Goswami, B.S. Tomar, J. Phys. G, Nucl. Part. Phys. 29 (2003) 1011.
[5] D. Singh, Rahbar Ali, M. Afzal Ansari, B.S. Tomar, M.H. Rashid, R. Guin, S.K. Das, Nucl. Phys. A 879 (2012) 107;
D. Singh, Rahbar Ali, M. Afzal Ansari, B.S. Tomar, M.H. Rashid, R. Guin, S.K. Das, Phys. Rev. C 79 (2009) 054601.
[6] D. Singh, R. Ali, M. Afzal Ansari, B.S. Tomar, M.H. Rashid, R. Guin, S.K. Das, Phys. Rev. C 83 (2011) 054604.
[7] Rahbar Ali, D. Singh, M. Afzal Ansari, M.H. Rashid, R. Guin, S.K. Das, J. Phys. G, Nucl. Part. Phys. 37 (2010) 115101.
[8] Harold C. Britt, Arthur R. Quinton, Phys. Rev. 124 (1961) 877.
[9] T. Inamura, M. Ishihara, T. Fukuda, T. Shimoda, H. Hiruta, Phys. Lett. B 68 (1977) 51.
[10] Claudie Gerschel, Nucl. Phys. A 387 (1982) 297.
[11] T. Udagawa, T. Tamura, Phys. Rev. Lett. 45 (1980) 1311.
[12] J. Wilczynski, K. Siwek-Wilczynska, J. Van-Driel, S. Gonggrijp, D.C.J.M. Hageman, R.V.F. Janssens, J. Lukasiak, R.H. Siemssen, S.Y. Van Der Werf, Nucl. Phys. A 373 (1982) 109.
[13] J.P. Bondorf, J.N. De, G. Fai, A.O.T. Karvinen, B. Jakobsson, J. Randrup, Nucl. Phys. A 333 (1980) 285.
[14] M.I. Sobel, P.J. Siemens, J.P. Bondrof, H.A. Bethe, Nucl. Phys. A 251 (1975) 502.
[15] V. Zagrebaev, Y. Penionzhkevich, Prog. Part. Nucl. Phys. 35 (1995) 575.
[16] H. Tricoire, C. Gerschel, A. Gillibert, N. Perrin, Z. Phys. A, At. Nucl. 323 (1986) 163.
[17] Kamal Kumar, Tauseef Ahmad, Sabir Ali, I.A. Rizvi, Avinash Agarwal, R. Kumar, K.S. Golda, A.K. Chaubey, Phys. Rev. C 87 (2013) 044608.
[18] Harish Kumar, Suhail A. Tali, M. Afzal Ansari, D. Singh, Rahbar Ali, Kamal Kumar, N.P.M. Sathik, Siddharth Parashari, Asif Ali, R. Dubey, Indu Bala, Rakesh Kumar, R.P. Singh, S. Muralithar, Nucl. Phys. A 960 (2017) 53.
[19] D.J. Parker, J.J. Hogan, J. Asher, Phys. Rev. C 39 (1989) 2256.
[20] H. Morgenstern, W. Bohne, W. Galster, K. Grabisch, A. Kyanowski, Phys. Rev. Lett. 52 (1984) 1104.
[21] Mohd Shuaib, Vijay R. Sharma, Abhishek Yadav, Pushpendra P. Singh, Manoj Kumar Sharma, Devendra P. Singh, R. Kumar, S. Muralithar, B.P. Singh, R. Prasad, Phys. Rev. C 94 (2016) 014613.
[22] O.B. Tarasov, D. Bazin, Nucl. Instrum. Methods Phys. Res., Sect. B 266 (2008) 4657–4664;
A. Gavron, Phys. Rev. C 21 (1980) 230–236;
http://lise.nscl.msu.edu/pace4.
[23] D. Singh, M. Afzal Ansari, R. Ali, N.P.M. Sathik, M. Ismail, J. Phys. Soc. Jpn. 82 (2013) 104201.
[24] J.F. Ziegler, SRIM08, The Stopping and Range of Ions in Matter, 2008, http://www.srim.org/.
[25] P.M. Strudler, I.L. Preiss, Richard Wolfgang, Phys. Rev. 154 (1967) 1126.
[26] CANDLE – Data Acquisition and Analysis System Designed to Support the Accelerator Based Experiments at Inter University Accelerator Center (IUAC), New Delhi, India.
[27] S.Y.F. Chu, L.P. Ekstrom, R.B. Firestone, The Lund/LBNL Nuclear Data Search, LBNL, Berkeley, USA, Version 2.0, 1999, http://nucleardata.nuclear.lu.se/toi/index.asp.
[28] National Nuclear Data Centre, Brookhaven National Laboratory, https://www.nndc.bnl.gov/chart.
[29] M. Afzal Ansari, R.K. Yaiskul Singh, M.L. Sehgal, V.K. Mittal, D.K. Avasthi, I.M. Govil, Ann. Nucl. Energy 11 (1984) 173.
[30] M. Cavinato, E. Fabrici, E. Gadioli, E. Gadioli Erba, P. Vergani, M. Crippa, G. Colombo, I. Redaelli, M. Ripamonti, Phys. Rev. C 52 (1995) 2577.
[31] R. Bass, Nucl. Phys. A 231 (1974) 45.
[32] Abhishek Yadav, Vijay R. Sharma, Pushpendra P. Singh, R. Kumar, D.P. Singh, Unnati, M.K. Sharma, B.P. Singh, R. Prasad, Phys. Rev. C 86 (2012) 014603.
[33] Vijay R. Sharma, Abhishek Yadav, Pushpendra P. Singh, Devendra P. Singh, Sunita Gupta, M.K. Sharma, Indu Bala, R. Kumar, S. Murlithar, B.P. Singh, R. Prasad, Phys. Rev. C 89 (2014) 024608.
[34] Kamal Kumar, Tauseef Ahmad, Sabir Ali, I.A. Rizvi, Avinash Agarwal, R. Kumar, A.K. Chaubey, Phys. Rev. C 88 (2013) 064613.
[35] Devendra P. Singh, Vijay R. Sharma, Abhishek Yadav, Pushpendra P. Singh, Unnati, M.K. Sharma, B.P. Singh, R. Prasad, Phys. Rev. C 89 (2014) 024612.
[36] Manoj Kumar Sharma, Unnati, B.P. Singh, Rakesh Kumar, K.S. Golda, H.D. Bhardwaj, R. Prasad, Nucl. Phys. A 776 (2006) 83.

[37] Sunita Gupta, B.P. Singh, M.M. Musthafa, H.D. Bhardwaj, R. Prasad, Phys. Rev. C 61 (2000) 064613.
[38] Pushpendra P. Singh, B.P. Singh, Manoj Kumar Sharma, Unnati, Devendra P. Singh, R. Prasad, Rakesh Kumar, K.S. Golda, Phys. Rev. C 77 (2008) 014607.
[39] S. Chakrabarty, B.S. Tomar, A. Goswami, G.K. Gubbi, S.B. Manohar, Anil Sharma, B. Bindukumar, S. Mukherjee, Nucl. Phys. A 678 (2000) 355.
[40] Abhishek Yadav, Vijay R. Sharma, Pushpendra P. Singh, Devendra P. Singh, Manoj K. Sharma, Unnati Gupta, R. Kumar, B.P. Singh, R. Prasad, R.K. Bhowmik, Phys. Rev. C 85 (2012) 034614.
[41] S. Mukherjee, A. Sharma, S. Sodaye, A. Gowswami, B.S. Tomar, Int. J. Mod. Phys. E 15 (2006) 237.
[42] B. Bindu Kumar, Anil Sharma, S. Mukherjee, S. Chakrabarty, P.K. Pujari, B.S. Tomar, A. Goswami, S.B. Manohar, S.K. Datta, Phys. Rev. C 59 (1999) 2923.